Rapid Communications

Spin-gap and two-dimensional magnetic excitations in Sr_2IrO_4

S. Calder,[1,*] D. M. Pajerowski,[1] M. B. Stone,[1] and A. F. May[2]

[1]*Neutron Scattering Division, Oak Ridge National Laboratory, Oak Ridge, Tennessee 37831, USA*

[2]*Materials Science and Technology Division, Oak Ridge National Laboratory, Oak Ridge, Tennessee 37831, USA*

(Received 31 August 2018; revised manuscript received 26 October 2018; published 4 December 2018)

Time-of-flight inelastic neutron scattering measurements on Sr_2IrO_4 single crystals were performed to access the spin Hamiltonian in this canonical $J_{\rm eff} = 1/2$ spin-orbital Mott insulator. The momentum of magnetic scattering at all inelastic energies measured is revealed to be L independent, indicative of idealized two-dimensional in-plane correlations. We model the in-plane energy and momentum dependence of the excitations, that were measured up to ∼80 meV, and define a spin gap of 0.6(1) meV. Collectively, the results indicate that despite the strongly spin-orbit entangled isospins, an isotropic two-dimensional $S = 1/2$ Heisenberg model Hamiltonian accurately describes the magnetic interactions, confirming a robust analogy with unconventional superconducting cuprates.

DOI: 10.1103/PhysRevB.98.220402

In $5d$ oxides the presence of large spin-orbit coupling (SOC), an appreciable Coulomb interaction (U), and large orbital hybridization produces strongly correlated behavior [1–3]. These behaviors include exotic quasiparticles such as Majorana fermions and quantum spin-liquid phenomena, Weyl fermions, magnetism with strong bond directionality and lattice coupling, and unusual insulating states [4–8]. The increased focus on $5d$ materials stems from the observation that relativistic SOC drives a Mott-like insulating ground state with pseudospin $J_{\rm eff} = 1/2$ magnetic moments in the iridate compound Sr_2IrO_4 [9,10]. While the list of interesting $5d$ compounds continues to grow, Sr_2IrO_4 endures as a canonical material.

One surprising aspect of the physics of Sr_2IrO_4 is the similarities to the parent unconventional cuprate La_2CuO_4. The degree to which this analogy holds stands as an important outstanding question with broad implications on a wide sphere of condensed matter physics. Compelling evidence for the proximity of Sr_2IrO_4 to an unconventional superconducting state analogous to that in the cuprates was observed in the measurements of the energy and momentum dependence of magnetic excitations in Sr_2IrO_4 with resonant inelastic x-ray scattering (RIXS) [11]. As with the parent cuprate La_2CuO_4, an isotropic two-dimensional (2D) Heisenberg model described the measured region of the excitation spectra of Sr_2IrO_4. This was in contrast to an initial theoretical consideration predicting highly anisotropic (gapped) behavior [12], however, given the 130 meV resolution, the low-energy regime could not be adequately accessed. Nevertheless, coupled with similarities of the ground-state properties between Sr_2IrO_4 and La_2CuO_4 in terms of the layered perovskite crystal structure, antiferromagnetic ordering of pseudospin-1/2 moments, Mott insulating behavior, and signatures associated with superconductivity on the surface of doped Sr_2IrO_4 provide an intriguing case [10,13–16]. These observations have led to many open questions regarding the extent to the similarities, in particular, when discussing model Hamiltonians.

Of central importance is determining how the strong SOC affects the magnetic excitations in Sr_2IrO_4. There is an expected appreciable impact of SOC on the magnetic moments of Sr_2IrO_4 ($\lambda_{\rm SO}$[Ir] ≈ 0.7 eV) while conversely being essentially negligible in La_2CuO_4 ($\lambda_{\rm SO}$[Cu] ≈ 0.01 eV). For example, this strong SOC limit in Sr_2IrO_4 is manifested in the rigid canting of the Ir moments due to the Dzyaloshinskii-Moriya (DM) interaction [17]. This is at odds to the analogous magnetic excitations in Sr_2IrO_4 and La_2CuO_4 suggested from RIXS [11]. Considering the magnetic interactions in Sr_2IrO_4, the dominant part of the magnetic Hamiltonian in the weak SOC limit is isotropic, but the introduction of SOC and Hund's coupling results in anisotropic terms [12], with debate as to which regime Sr_2IrO_4 resides.

Experimentally, the presence or absence of an energy gap in the magnetic excitation spectra at the magnetic zone center (π, π) delineates between isotropic or anisotropic interactions [12]. Conflicting reports, however, on the low-energy excitations have resulted in debate as to whether the collective excitations in Sr_2IrO_4 differ from cuprates. While the initial RIXS measurements in Ref. [11] did not allow suitable access to this low-energy regime, subsequent studies with an improved resolution of 30 meV have found either no indication of a spin gap [18,19] or, conversely, strongly gapped excitations of the order 20–30 meV [20,21]. Separate, less direct measurements using electron spin resonance (ESR) and Raman scattering have indicated field-dependent gaps of ∼1 meV, however, these were extracted from applied field measurements above the critical field ($H > 0.2$ T [10]) that alters the magnetic structure from the zero-field ground state [22,23]. This introduces some ambiguity since RIXS measurements of doped Sr_2IrO_4, that also show altered magnetic structures, indicate the magnetic excitations can be strongly renormalized as the magnetic structure is altered [18,19,24,25]. Moreover, no measurement has directly shown that the out-of-plane interactions

*caldersa@ornl.gov

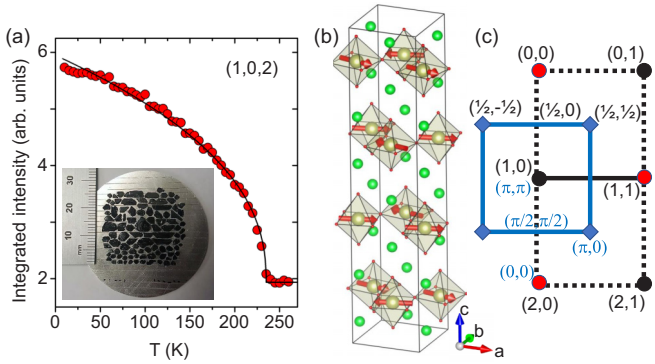

FIG. 1. Sr_2IrO_4 crystal structure and magnetic ordering. (a) The single-crystal array of Sr_2IrO_4 and measurement of magnetic ordering of the (1,0,2) reflection. The data (circles) are fit to a power law (line), with $T_N = 240$ K. (b) Crystal and magnetic structure of Sr_2IrO_4. (c) Structural (red circles) and magnetic (black circles) reciprocal space. High-symmetry magnetic zone boundary points are indicated by the blue diamonds. H and K points are labeled along with the labeling in the square lattice notation used to describe the dispersions. The square lattice is rotated from the conventional lattice of Sr_2IrO_4.

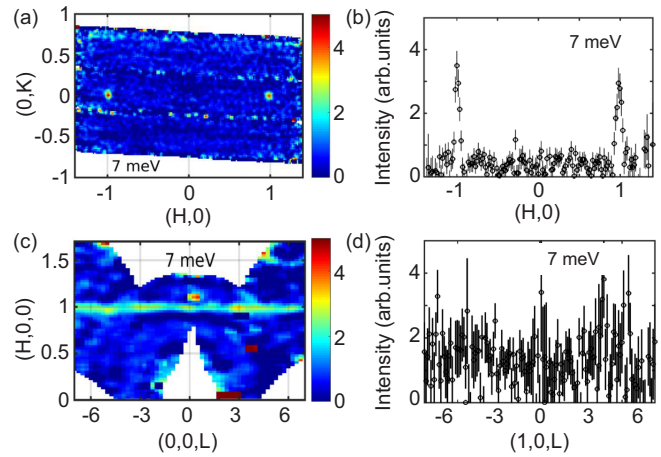

FIG. 2. Time-of-flight inelastic neutron scattering measurements of Sr_2IrO_4 on SEQUOIA. (a) The magnetic excitations around (π, π) are shown in the (H, K) plane at $E = 7$ meV. (b) Cut along $(H, 0)$ over a K range of $[-0.05, 0.05]$ and $L = [-5, 5]$, showing sharp inelastic peaks at $(-1, 0)$ and $(1,0)$. (c) Inelastic scattering in the $(H, 0, L)$ plane at $E = 7$ meV. (d) Cut along the rod of scattering at $(1, 0, L)$ with a K and H range of $[-0.075, 0.075]$.

are negligible and the assumption of a 2D Hamiltonian is robust.

Here, we present time-of-flight inelastic neutron scattering (INS) measurements that directly access the low-energy magnetic excitation spectra and reveal the dimensionality of the correlations. In general, INS has unique capabilities in probing magnetic excitations, with the measurements corresponding to a well understood $S(Q, \omega)$ scattering cross section. Moreover, the use of time-of-flight neutrons from spallation sources, coupled with instruments containing large detector arrays, allows ready access to large maps of four-dimensional (H, K, L, E) reciprocal space. The energy resolution of neutron spectrometers additionally cover the eV down to meV energy regime, allowing the full mapping of high-energy excitations as well as the unambiguous inspection of low-energy scattering to high precision. As such, INS has proven irreplaceable in the study of the cuprates [26] and measurements on Sr_2IrO_4 have been a long-standing goal.

Sr_2IrO_4, however, offers technical challenges for INS measurements. Hurdles include the strong neutron absorption of iridium, small ordered moment sizes ($0.2\mu_B$–$0.3\mu_B$), rapidly falling off intensity with Q due to the Ir magnetic form factor, and small crystal sizes that together hinder the detection of magnetic signals. To overcome these issues we prepared an array of ~100 single crystals of Sr_2IrO_4 with a total mass of 1.1 g, shown in Fig. 1(a). The largest single crystal of Sr_2IrO_4 was 300 mg, representing more than an order of magnitude increase in size compared to previous reports in the literature [14,15,27]. Crystals were grown in several batches and were found to consistently have the same ordering temperature of 240 K associated with nondeficient Sr_2IrO_4 crystals [27,28]. The array was aligned in the $[H0L]$ horizontal scattering plane using a backscattering x-ray Laue and subsequent measurements with neutrons found a mosaic of 2° full width at half maximum (FWHM). The magnetic ordering temperature of the full array was probed with the fixed elastic energy triple axis neutron spectrometer HB-1A at the High Flux Isotope Reactor (HFIR). The magnetic order of the full array was confirmed to occur at 240 K by following the intensity of the magnetic (1,0,2) reflection as shown in Fig. 1(a).

The INS measurements covered an energy up to ~100 meV and were performed on the SEQUOIA and CNCS time-of-flight spectrometers at the Spallation Neutron Source, ORNL [29]. An incident energy of 3.32 meV was utilized on CNCS to access the scattering at (π, π) and define the spin gap. The elastic line instrumental resolution of this instrument was fit to 0.1 meV. The chosen E_i offers a low background since it is below the Al cutoff energy, mitigating Bragg scattering from the sample environment and Al crystal mount. On SEQUOIA, measurements were performed with incident energies of $E_i = 20$, 60, and 120 meV. On both instruments, measurements were taken at fixed angles from $\psi = \pm 30°$, with $\psi = 0$ corresponding to the incident neutron beam (k_i) being parallel to the crystallographic c axis. This rotation range allowed coverage of a large volume of reciprocal space while negating neutron absorption. On SEQUOIA data were collected under the same conditions using an empty sample holder and identical Al disk with a similar mass of Fomblin grease to subtract out the background scattering. All INS measurements were performed at 10 K in the ordered state.

The INS data directly show that the magnetic correlations in Sr_2IrO_4 are highly 2D in nature. The antiferromagnetic order of Sr_2IrO_4 yields magnetic scattering at $10L$ (L = even) Bragg reflections. These elastic reflections are narrow along both the in-plane (H, K) and out-of-plane L directions. In the INS data, sharp inelastic excitations are observed from the (π, π) magnetic zone center [Figs. 2(a) and 2(b)]. Conversely, the magnetic excitations are rods of scattering along the $(1, 0, L)$ direction [Figs. 2(c) and 2(d)], with no observable momentum dependence along the L direction. This

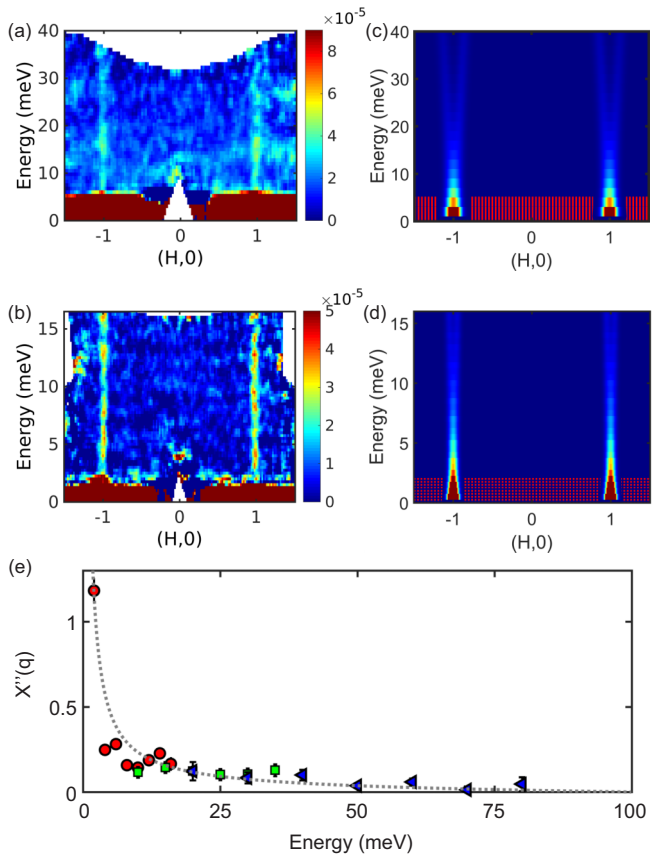

FIG. 3. Inelastic neutron scattering data measured on SEQUOIA for (a) $E_i = 60$ meV and (b) $E_i = 20.5$ meV. (c), (d) These are compared with model calculations of spin-wave excitations using Eq. (1) convoluted with the appropriate instrument energy resolution for each E_i. (e) Extracted intensity of the inelastic scattering for $E_i =$ 20 meV (circle), $E_i = 60$ meV (square), $E_i = 120$ meV (triangle). The intensities have been scaled to account for flux differences with the different incident energies. The dashed line is the calculated scattering intensity of the excitation as a function of energy transfer. The largest scattering intensity occurs near the (π, π) point (0 meV) and the minimum scattering intensity is at the (0,0) wave vector and top of the excitation band (100 meV).

L behavior was observed over the fully measured inelastic energy range, providing direct experimental evidence that the magnetic correlations are 2D. Therefore, the INS results show that utilizing a 2D Heisenberg model is applicable in Sr_2IrO_4. Additionally, the lack of L dispersion offers the powerful analysis avenue of being able to integrate the data over a large L range to access wider in-plane coverage at higher statistics (signal to noise). This integration is extremely beneficial to time-of-flight INS that yields large volumes of (H, K, L, E) space which can then be appropriately integrated to increase access to the in-plane magnetic spectrum. It was checked that integrating over L produced identical results to only utilizing a narrow L range.

Intermediate incident energies, using $E_i = 20.5$ and 60 meV, show spin excitations with intensity that is clearly present down to 2 meV [Figs. 3(a) and 3(b)]. Sharp scattering is observed from (π, π) that broadens and decreases in intensity as it extends up to high energy. By inspection of Fig. 3(b) there is no observable spin gap within the 2 meV resolution. Therefore, before focusing on lower-energy measurements, we begin by utilizing the isotropic 2D Heisenberg model with $S = 1/2$,

$$\mathcal{H} = \sum_{i,j} J_{ij} \vec{S}_i \cdot \vec{S}_j + \Gamma S_i^z S_i^z + D\left(S_i^x \cdot S_j^y - S_i^y S_j^x\right), \quad (1)$$

with J corresponding to the isotropic magnetic exchange interaction in the plane, Γ corresponding to the symmetric exchange anisotropy, and D antisymmetric exchange anisotropy. The two exchange anisotropies compete, with Γ facilitating collinear c-axis spins and D promoting in-plane canting. The values for nearest-neighbor Heisenberg exchange have been found from previous RIXS studies of $J_1 = 57$ meV, $J_2 = -16$ meV, and $J_3 = 12$ meV, and these are utilized in the analysis of the INS data [10,18,21]. Given the lack of any observed spin gap in the data in Fig. 3, we begin by using a zero-gap model.

Good agreement is seen between the measured and calculated dispersion maps in Figs. 3(a)–3(d). To further test this model, constant energy cuts of the data were taken and the scattered intensity fit to a Gaussian centered on (1,0) for $E_i = 20.5$ meV (energy cut range of ± 2 meV), 60 meV (energy cut range of ± 5 meV), and 120 meV (energy cut range of ± 10 meV) [see Fig. 3(e)]. The different E_i experimental setups have different incident flux and so each E_i data set was normalized at overlapping inelastic energies. The INS data covered the dispersion region from (π, π) to (0,0). The calculated intensity $\chi''(q)$ from Eq. (1) closely follows the extracted intensity from the INS data. The agreement of the dispersion and intensity, that can be directly compared to INS measurements, provides strong evidence for the applicability of an isotropic pseudo $S = 1/2$ 2D Heisenberg model.

Having established the existence of magnetic scattering down to 2 meV resolution, we consider excitations emanating from the zone center (π, π), measured with a resolution of 0.1 meV, to define the spin gap. The high-resolution results are shown in Fig. 4. The in-plane scattering, integrated over an L range of ± 2.5, shows well-defined scattering centered on (1,0) [see Fig. 4(a)]. The measured dispersion [Fig. 4(b)] at various energy transfers shows scattering at (π, π) well below 2 meV. To extract quantitative information, constant energy cuts, with a range of ± 0.15 meV, along the $(H, 0)$ direction are taken and these are fit to a Gaussian peak shape centered on (1,0). The cuts and fits are shown in Fig. 4(c). The increased background in going from 2.25 to 0 meV, neglecting the elastic line, can be attributed to incoherent scattering from the Fomblin grease, observable in Fig. 4(b). We extracted a constant fitted flat background from the data for each energy to produce the plots in Fig. 4(c). The corresponding intensity as a function of energy is shown in Fig. 4(e), with values going to zero intensity at the lowest energy indicating a finite spin gap. To extract the spin-gap value, we then modeled the low-energy scattering using Eq. (1) with anisotropy introduced. Using the instrument resolution, the calculated intensity variation with energy was obtained. The model intensity at (1,0) was then compared to the extracted intensity from the data, with the best match shown in Fig. 4(e). To define the spin-gap

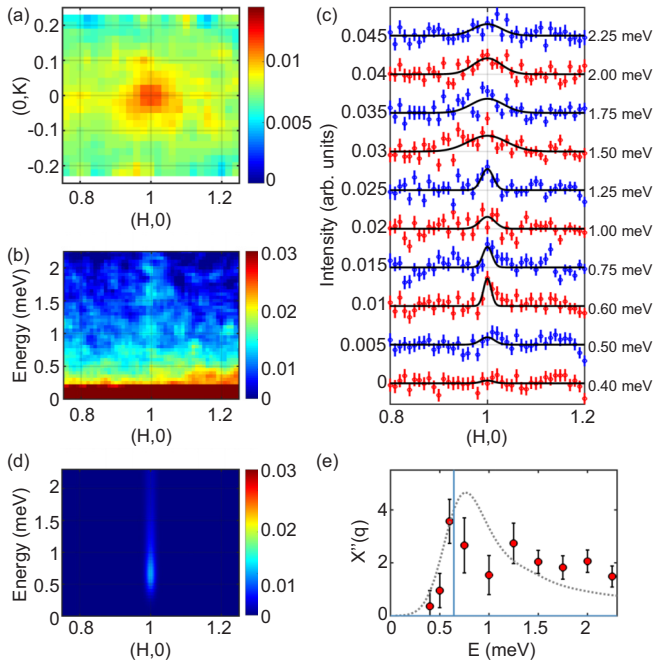

FIG. 4. Measurements of Sr_2IrO_4 with cold neutrons ($E_i = 3.32$ meV) on the CNCS. (a) Scattering centered at (π, π) is shown at 1.5 meV over an energy range of ± 0.25 meV and L range of $[-2.5, 2.5]$. (b) The low-energy dispersion from (π, π) is shown. The K range is $[-0.025, 0.025]$ and L range is $[-2.5, 2.5]$. (c) Cuts along $(H, 0)$ down to 0.4 meV with a K range of $[-0.05, 0.05]$, L range of $[-2.5, 2.5]$, and energy range of ± 0.15 meV. The black lines are Gaussian fits centered on (1,0). Each energy is offset by a constant factor of 5×10^{-3}. (d) Calculated low-energy scattering. (e) The extracted intensity from Gaussian fits at various energies (circles) is compared to the model intensity variation with energy, including instrument resolution, at (π, π) (dotted line). The solid line is the modeled spectra with no instrument resolution that provides a sharp peak at the spin-gap energy.

energy, the instrumental resolution was removed from the model, with the consequence of producing a sharp Dirac delta peak at a single energy, shown by the solid line in Fig. 4(e). This allows a spin-gap definition of 0.6(1) meV. These results with INS therefore provide definitive evidence of the zero-field spin gap and should serve to resolve the debate in the literate.

From the INS results, Sr_2IrO_4 can be placed in the weak-to-intermediate SOC limit. Given the large magnetic excitation bandwidth of 200 meV, the spin gap is finite but negligible. For comparison, the measured spin gap in La_2CuO_4 from INS is 5 meV, with an excitation bandwidth of 300 meV, despite the order of magnitude reduced SOC in Cu compared to Ir. This is surprising considering the importance of SOC in generating the electronic ground state in Sr_2IrO_4, however, the results indicate a dramatically reduced impact of SOC on the manifested magnetic correlations. The Ir^{4+} ion has $\lambda_{SO} = 0.7$ eV in Sr_2IrO_4 and the crystal field splitting is $\Delta_{oct} = 3.5$ eV [30], placing Sr_2IrO_4 in the intermediate-coupling limit. With the tetragonal distortion of the oxygen coordination sphere, the first excited state in the strong crystal field picture, as found in cuprates, then is strongly mixed with the ground state and gives an easy plane anisotropy that makes the system quasi-2D and is the manifestation of the large SOC. Then there exists a slight rhombic term in the plane, along the b axis [31], that produces the small but finite measured gap. The small gap, and therefore small anisotropy, coupled with the measurement of 2D correlations in Figs. 2(c) and 2(d) indicates an isotropic 2D model will robustly describe magnetic correlations in Sr_2IrO_4.

Collectively, the results presented provide compelling evidence for the mapping of the physics of Sr_2IrO_4 onto the parent cuprate La_2CuO_4. While the high-energy spin excitations have been followed with RIXS, the intensity of the scattering cross section measured is not fully described. Therefore the similarities of the RIXS data and the INS measurements are in some respects remarkable. These results in themselves provide a system-independent verification of the quantitative data available from RIXS at high energies and show the power of combining results from RIXS and INS in $5d$-based materials. In this case the limitation of RIXS is the energy resolution, although strong advances have been made [32]. INS, therefore, offers the unparalleled ability to probe low-energy sub-meV signals over the full reciprocal space. This has allowed the definition of the small spin-gap energy in Sr_2IrO_4, resolving contradictory reports from various techniques, and shown 2D magnetic correlations.

In conclusion, the in-plane spin-gap of Sr_2IrO_4 is measured to be 0.6(1) meV and the magnetic correlations shown to be highly two dimensional. These results were obtained through inelastic neutron scattering measurements performed on single crystals of Sr_2IrO_4 within the magnetically order phase. Well-defined excitations were revealed using high-resolution measurements to give a spin-gap value. The excitation spectrum is found to be strongly two dimensional with no measurable out-of-plane dispersion. Collectively, the INS measurements show that an isotropic $S = 1/2$ 2D Heisenberg model describes the general physics of the magnetic interactions in Sr_2IrO_4. The implications reinforce the analogy with cuprates despite the presence of strong SOC on the Ir ion that would be expected to result in anisotropic behavior.

The Department of Energy will provide public access to these results of federally sponsored research in accordance with the DOE Public Access Plan [33].

This research used resources at the High Flux Isotope Reactor and Spallation Neutron Source, a DOE Office of Science User Facility operated by the Oak Ridge National Laboratory. Sample synthesis and characterization (AFM) was supported by the U.S. Department of Energy, Office of Science, Basic Energy Sciences, Materials Sciences and Engineering Division. We acknowledge W. Tian and A. I. Kolesnikov for assistance during the neutron measurements. ORNL is managed by UT-Battelle, LLC, under Contract No. DE-AC05-00OR22725 with the U.S. Department of Energy. The U.S. Government retains, and the publisher, by accepting the article for publication, acknowledges that the U.S. Government retains a nonexclusive, paid-up, irrevocable, worldwide license to publish or reproduce the published form of this manuscript, or allow others to do so, for U.S. Government purposes.

[1] D. Pesin and L. Balents, Nat. Phys. **6**, 376 (2010).

[2] J. G. Rau, E. K.-H. Lee, and H.-Y. Kee, Annu. Rev. Condens. Matter Phys. **7**, 195 (2016).

[3] W. Witczak-Krempa, G. Chen, Y. B. Kim, and L. Balents, Annu. Rev. Condens. Matter Phys. **5**, 57 (2014).

[4] S. K. Choi, R. Coldea, A. N. Kolmogorov, T. Lancaster, I. I. Mazin, S. J. Blundell, P. G. Radaelli, Y. Singh, P. Gegenwart, K. R. Choi, S.-W. Cheong, P. J. Baker, C. Stock, and J. Taylor, Phys. Rev. Lett. **108**, 127204 (2012).

[5] S. H. Chun, J.-W. Kim, J. Kim, H. Zheng, C. C. Stoumpos, C. D. Malliakas, J. F. Mitchell, K. Mehlawat, Y. Singh, Y. Choi, T. Gog, A. Al-Zein, M. M. Sala, M. Krisch, J. Chaloupka, G. Jackeli, G. Khaliullin, and B. J. Kim, Nat. Phys. **11**, 462 (2015).

[6] Q. Cui, J.-G. Cheng, W. Fan, A. E. Taylor, S. Calder, M. A. McGuire, J.-Q. Yan, D. Meyers, X. Li, Y. Q. Cai, Y. Y. Jiao, Y. Choi, D. Haskel, H. Gotou, Y. Uwatoko, J. Chakhalian, A. D. Christianson, S. Yunoki, J. B. Goodenough, and J.-S. Zhou, Phys. Rev. Lett. **117**, 176603 (2016).

[7] K. Kitagawa, T. Takayama, Y. Matsumoto, A. Kato, R. Takano, Y. Kishimoto, S. Bette, R. Dinnebier, G. Jackeli, and H. Takagi, Nature (London) **554**, 341 (2018).

[8] M. Majumder, R. S. Manna, G. Simutis, J. C. Orain, T. Dey, F. Freund, A. Jesche, R. Khasanov, P. K. Biswas, E. Bykova, N. Dubrovinskaia, L. S. Dubrovinsky, R. Yadav, L. Hozoi, S. Nishimoto, A. A. Tsirlin, and P. Gegenwart, Phys. Rev. Lett. **120**, 237202 (2018).

[9] B. J. Kim, H. Jin, S. J. Moon, J.-Y. Kim, B.-G. Park, C. S. Leem, J. Yu, T. W. Noh, C. Kim, S.-J. Oh, J.-H. Park, V. Durairaj, G. Cao, and E. Rotenberg, Phys. Rev. Lett. **101**, 076402 (2008).

[10] B. J. Kim, H. Ohsumi, T. Komesu, S. Sakai, T. Morita, H. Takagi, and T. Arima, Science **323**, 1329 (2009).

[11] J. Kim, D. Casa, M. H. Upton, T. Gog, Y.-J. Kim, J. F. Mitchell, M. van Veenendaal, M. Daghofer, J. van den Brink, G. Khaliullin, and B. J. Kim, Phys. Rev. Lett. **108**, 177003 (2012).

[12] G. Jackeli and G. Khaliullin, Phys. Rev. Lett. **102**, 017205 (2009).

[13] M. K. Crawford, M. A. Subramanian, R. L. Harlow, J. A. Fernandez-Baca, Z. R. Wang, and D. C. Johnston, Phys. Rev. B **49**, 9198 (1994).

[14] F. Ye, S. Chi, B. C. Chakoumakos, J. A. Fernandez-Baca, T. Qi, and G. Cao, Phys. Rev. B **87**, 140406 (2013).

[15] C. Dhital, T. Hogan, Z. Yamani, C. de la Cruz, X. Chen, S. Khadka, Z. Ren, and S. D. Wilson, Phys. Rev. B **87**, 144405 (2013).

[16] Y. K. Kim, O. Krupin, J. D. Denlinger, A. Bostwick, E. Rotenberg, Q. Zhao, J. F. Mitchell, J. W. Allen, and B. J. Kim, Science **345**, 187 (2014).

[17] S. Boseggia, H. C. Walker, J. Vale, R. Springell, Z. Feng, R. S. Perry, M. M. Sala, H. M. Rnnow, S. P. Collins, and D. F. McMorrow, J. Phys.: Condens. Matter **25**, 422202 (2013).

[18] H. Gretarsson, N. H. Sung, J. Porras, J. Bertinshaw, C. Dietl, J. A. N. Bruin, A. F. Bangura, Y. K. Kim, R. Dinnebier, J. Kim, A. Al-Zein, M. Moretti Sala, M. Krisch, M. Le Tacon, B. Keimer, and B. J. Kim, Phys. Rev. Lett. **117**, 107001 (2016).

[19] X. Liu, M. P. M. Dean, Z. Y. Meng, M. H. Upton, T. Qi, T. Gog, Y. Cao, J. Q. Lin, D. Meyers, H. Ding, G. Cao, and J. P. Hill, Phys. Rev. B **93**, 241102 (2016).

[20] J. G. Vale, S. Boseggia, H. C. Walker, R. Springell, Z. Feng, E. C. Hunter, R. S. Perry, D. Prabhakaran, A. T. Boothroyd, S. P. Collins, H. M. Rønnow, and D. F. McMorrow, Phys. Rev. B **92**, 020406 (2015).

[21] D. Pincini, J. G. Vale, C. Donnerer, A. de la Torre, E. C. Hunter, R. Perry, M. Moretti Sala, F. Baumberger, and D. F. McMorrow, Phys. Rev. B **96**, 075162 (2017).

[22] S. Bahr, A. Alfonsov, G. Jackeli, G. Khaliullin, A. Matsumoto, T. Takayama, H. Takagi, B. Büchner, and V. Kataev, Phys. Rev. B **89**, 180401 (2014).

[23] Y. Gim, A. Sethi, Q. Zhao, J. F. Mitchell, G. Cao, and S. L. Cooper, Phys. Rev. B **93**, 024405 (2016).

[24] S. Calder, J. W. Kim, A. E. Taylor, M. H. Upton, D. Casa, G. Cao, D. Mandrus, M. D. Lumsden, and A. D. Christianson, Phys. Rev. B **94**, 220407 (2016).

[25] Y. Cao, X. Liu, W. Xu, W.-G. Yin, D. Meyers, J. Kim, D. Casa, M. H. Upton, T. Gog, T. Berlijn, G. Alvarez, S. Yuan, J. Terzic, J. M. Tranquada, J. P. Hill, G. Cao, R. M. Konik, and M. P. M. Dean, Phys. Rev. B **95**, 121103 (2017).

[26] N. S. Headings, S. M. Hayden, R. Coldea, and T. G. Perring, Phys. Rev. Lett. **105**, 247001 (2010).

[27] N. H. Sung, H. Gretarsson, D. Proepper, J. Porras, M. L. Tacon, A. V. Boris, B. Keimer, and B. J. Kim, Philos. Mag. **96**, 413 (2016).

[28] E. J. Moon, A. F. May, P. Shafer, E. Arenholz, and S. J. May, Phys. Rev. B **95**, 155135 (2017).

[29] M. B. Stone, J. L. Niedziela, D. L. Abernathy, L. DeBeer-Schmitt, G. Ehlers, O. Garlea, G. E. Granroth, M. Graves-Brook, A. I. Kolesnikov, A. Podlesnyak, and B. Winn, Rev. Sci. Instrum. **85**, 045113 (2014).

[30] S. J. Moon, M. W. Kim, K. W. Kim, Y. S. Lee, J.-Y. Kim, J.-H. Park, B. J. Kim, S.-J. Oh, S. Nakatsuji, Y. Maeno, I. Nagai, S. I. Ikeda, G. Cao, and T. W. Noh, Phys. Rev. B **74**, 113104 (2006).

[31] M. Nauman, Y. Hong, T. Hussain, M. S. Seo, S. Y. Park, N. Lee, Y. J. Choi, W. Kang, and Y. Jo, Phys. Rev. B **96**, 155102 (2017).

[32] J. Kim, D. Casa, A. Said, R. Krakora, B. J. Kim, E. Kasman, X. Huang, and T. Gog, Sci. Rep. **8**, 1958 (2018).

[33] http://energy.gov/downloads/doepublic-access-plan.